In Situ Kinetics Study of the Accelerated Aging of Poly(ethylene oxide) Using PhotoDSC

F. Fraisse,[†] S. Morlat-Thérias,[†] J.-L. Gardette,[†] J.-M. Nedelec,[‡] and M. Baba*,[†]

Laboratoire de Photochimie Moléculaire et Macromoléculaire, UMR CNRS 6505, and Laboratoire des Matériaux Inorganiques, UMR CNRS 6002, Ecole Nationale Supérieure de Chimie de Clermont-Ferrand et Université Blaise Pascal, 24 Avenue des Landais, 63174 Aubière Cedex, France

Received: March 17, 2006; In Final Form: May 30, 2006

PhotoDSC has been applied to follow the global kinetics of chain scissions resulting from the UV light irradiation or from the thermal degradation of a high molecular weight PEO (4×10^6 g·mol^{-1}). Infrared spectroscopy, XRD measurements and rheology experiments were performed to evidence the occurrence of chain scissions. Melting energy was used as a tool to quantify the extent of the degradation. It was found that the chain scissions reaction follows a first-order kinetic law for both photo and thermal degradation. The activation energies were found identical in both cases (41 kJ·mol^{-1}), whereas the degradation rate was higher in the case of UV irradiation than in the case of thermoageing

Introduction

PhotoDSC combines in a single equipment light irradiation and DSC measurement. Light is brought inside the DSC furnace by two symmetrical optical fibers. Classically, photoDSC is devoted to photopolymerization studies. The heat released by the light/matter interactions is directly recorded by the DSC apparatus. In a previous paper[1] we demonstrated that the photoDSC system can be considered a very useful and versatile device for the in situ study of the aging of semicrystalline polymers. In fact, the possibility of easily controlling the temperature (−150 to 500 °C), the nature of the atmosphere (O_2, N_2, air, ...), the irradiation power (0−2000 mW), and the irradiation wavelength make this device an efficient tool to perform and characterize artificial accelerated photo and thermo degradation.

This paper presents a kinetic study of thermo and photoaging of poly(ethylene oxide), PEO, at several temperatures and light intensities. PEO is a semicrystalline water-soluble polymer,[2,3] with a crystallinity that is very sensitive to the thermal history of the samples,[4−6] which makes this property interesting as an indicator of the degradation.

Because it is a biodegradable and biocompatible polymer, PEO is a good candidate for environmental and medical applications.[7,8] The mechanisms of thermo and photooxidation of PEO have already been investigated[9,10] on the basis of IR identifications of the oxidation products. Interestingly, it was found that photooxidation favors the accumulation of formates against esters, whereas thermooxidation leads to equal amounts of both these oxidation products. It can be anticipated that both these conditions of aging result in different modifications of the macromolecular architecture since the formation of formates is accompanied by macromolecular chain scissions and the formation of esters is not.

The aim of this study is to show how photoDSC can be used to obtain kinetics constants and determine the thermodynamics properties associated to the degradation of a semicrystalline polymer such as PEO.

* To whom correspondence should be addressed. E-mail: mohamed.baba@univ-bpclermont.fr.
[†] Laboratoire de Photochimie Moléculaire et Macromoléculaire.
[‡] Laboratoire des Matériaux Inorganiques.

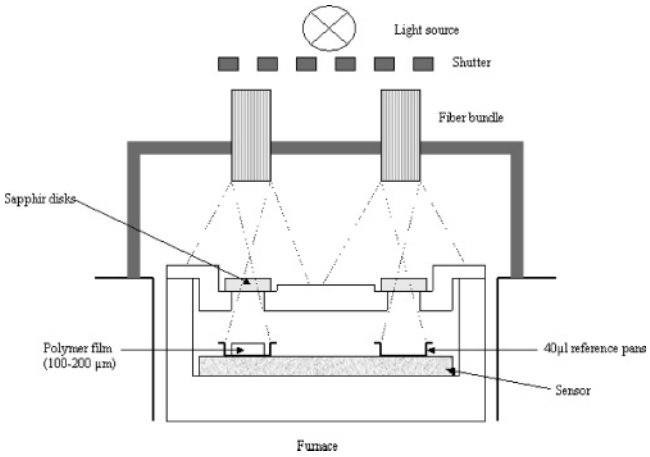

Figure 1. Principle of the photoDSC device.

Experimental Section

Several samples of poly(ethylene oxide) were used. The samples with a molecular weight (M_r) lower than 10^4 g·mol^{-1} are usually named PEG (poly(ethylene glycol)), whereas those with higher M_r were called PEO (poly(ethylene oxide)). PEGs and PEOs were supplied by Scientific Polymer Products. Table 1 gives their molecular weights.

A Mettler Toledo DSC822^e apparatus, equipped with an intracooler and a liquid nitrogen cooling set, was used. It allows working between 500 and −150 °C with a scanning temperature rate from 0.1 °C/h to 50 °C/min. Indium (156.61 °C), zinc (419.58 °C), and heptane (−90.61 °C) were used to calibrate this apparatus. A Hamamatsu light generator equipped with a "Lightningcure LC6" source (Xe/Hg, "medium pressure") was affixed to the DSC device as represented on Figure 1.

The light generator is servo-controlled by the DSC software (STARe) which permits a choice of both the light intensity from 0 to 324 mW/cm^2 and the duration of the irradiation. Two identical fiber bundles supply the irradiation light both to sample and reference DSC pans which are kept open. The source, filtered by the sapphire disks, delivers radiations of wavelengths longer than 300 nm, representative of outdoor aging.

All the experiments were performed under flowing air atmosphere (50 mL·min^{-1}).

10.1021/jp061669g CCC: $33.50
Published on Web 07/07/2006

TABLE 1: Molecular Weights of the PEG and PEO Samples Used

sample	PEO1	PEO2	PEG3	PEG4	PEG5	PEG6	PEG7	PEG8
M_r (g·mol^{-1})	4×10^6	10^5	10^4	8×10^3	4.6×10^3	2×10^3	1.5×10^3	4×10^2

X-ray diffraction (XRD) was performed on a Siemens D5000 diffractometer working in the Bragg−Brentano configuration with Cu Kα radiation ($\lambda = 1.5406$ Å). The use of a well-defined sample holder allowed reproducible quantitative measurements while keeping a constant analyzed volume for all samples.

Rheological measurements were carried out at 90 °C in isothermal conditions under air, by using an ARES rheometer (Rheometrics). Parallel plates with a diameter of 8 mm were used. A gap of 0.5 mm was adjusted between the plates. Storage modulus (G′) and loss modulus (G″) were recorded in oscillatory mode as a function of time for a 2% strain and a frequency of 3 rad·s^{-1}.

Films were prepared by pressure molding at 100 °C and under 19 Mpa for 1 min between two Teflon sheets, and they were analyzed by infrared spectrometry with a Nicolet 760-FTIR spectrometer, working with OMNIC software. The spectra were recorded using 32 scan summations and a 4 cm^{-1} resolution.

Results

1. Relationship Between the Crystallinity of the PEG and PEO Samples and Their Molecular Weight. To establish the relationship between the crystallinity of the PEG and PEO samples and their molecular weight, DSC and XRD experiments were performed and compared. Figure 2 shows the results of DSC recordings. For each sample, 10 mg were submitted to an appropriate program temperature to record the corresponding endotherm of fusion. The heating rate was taken equal to 2 °C/min. Both the heat of fusion (ΔH in J·g^{-1}), derived from the area under the peak, and the melting temperature (T_m), taken at the top of the signal, depend on the sample molecular weight (M_r). As can be seen in the inset, from 4×10^6 to 10^4 g·mol^{-1} ΔH increases whereas T_m remains quite constant. From 10^4 to 4×10^2 g·mol^{-1} both ΔH and T_m decrease continuously.

XRD patterns of the same samples are presented in Figure 3. The peak around 24° is a combination of the (112) and (032) reflections, and the peak at 20° corresponds to the (120) reflection.[11,12] The inset a presents an enlargement of the (120) peaks. In the inset b, the intensity of the (120) peaks was plotted versus the logarithm of M_r. Also, in the same inset (b), the interreticular distance (d) of the (120) plane was represented as function of log(M_r).

The intensity of the (120) reflection is obviously directly correlated with the level of crystallinity of the samples. It is indeed very striking to note that the evolution of the crystallinity with M_r is not monotonic since it first increases from 4×10^2 to 10^4 g·mol^{-1} and then continuously decreases for higher M_r. This complex behavior, which deserves further experiments to be fully explained, is indeed very well reproduced by the evolution of ΔH. It can be concluded by comparison of DSC and XRD data, that ΔH as measured by DSC is a good indicator of the crystallinity of the PEO samples.

Furthermore, as the chain length increases, the packing of the macromolecular chains is expected to be modified thus inducing a change of the structure of the crystalline part of the samples. These modifications are attested by the evolution of the interreticular distance d of the (120) plane as depicted in Figure 3b. The increase of d with M_r for low M_r is consistent with the increase of the chain length, but for higher M_r, the behavior is more complex indicating probably a structural rearrangement of the polymers chains. Once again it is indeed worthy to note that the complex evolution of d correlates very nicely with ΔH and the level of crystallinity. In conclusion, ΔH can be considered unambiguously as a quantitative indicator of the level of crystallinity of the PEO samples.

2. Photoaging of PEO. PEO1 sample (4×10^6 g·mol^{-1}) was submitted to photoaging using the photoDSC system. A small quantity around 6 mg of the PEO powder was set in the DSC pan and then exposed to the program described in Figure 4. The first stage consists of a thermal equilibration of the sample. It takes 1 min at the chosen temperature (90 °C for instance for the illustrated example) in the dark. Light was then switched on for a defined time (5 min in this example). During this time segment, photochemical modifications of the polymer occur as demonstrated by the shoulder observed five minutes after the beginning of the irradiation. The third segment allows the cooling of the sample. Switching off the light, the temperature was decreased from the isothermal aging temperature down to 0 °C at −2 °C·min^{-1}. The crystallization peak was recorded during this stage. From 0 °C, the sample was then heated to 90

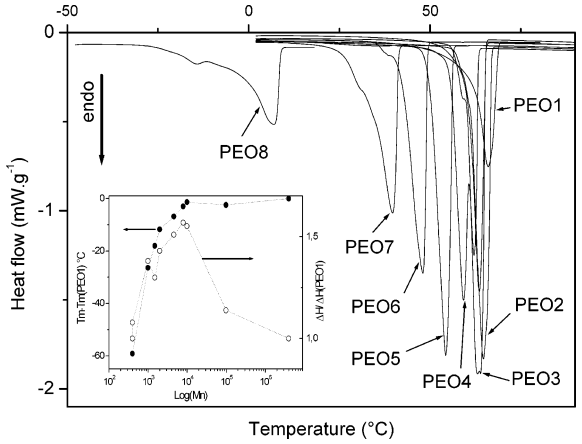

Figure 2. DSC endotherms of the fusion of PEOs samples (2 °C/min). PEO1−PEO8 correspond to the samples described in Table 1. In the inset are plotted the ratio of the heat of fusion of each sample to the heat of fusion of the higher molecular weight sample ($\Delta H/\Delta H$(PEO1); unshaded circle) and the shift of melting temperature ($T_m - T_m$(PEO1); shaded circle) as a function of molecular weight.

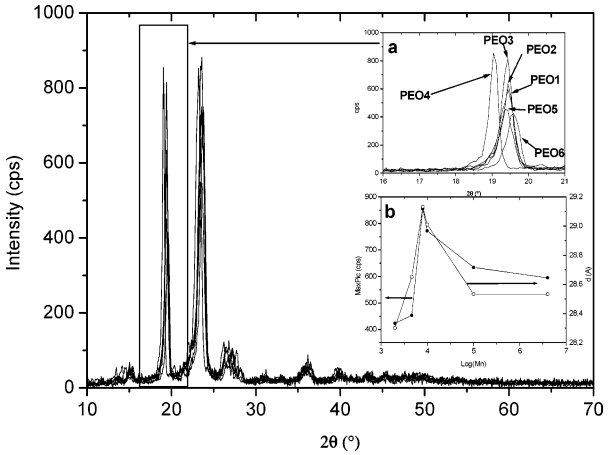

Figure 3. XRD patterns of PEG and PEO samples. Only the samples solid at room temperature were studied. Inset a is a zooming of the (120) peak. In the inset b, the (120) peak intensity and the interreticular distance (d) were plotted versus molecular weights.

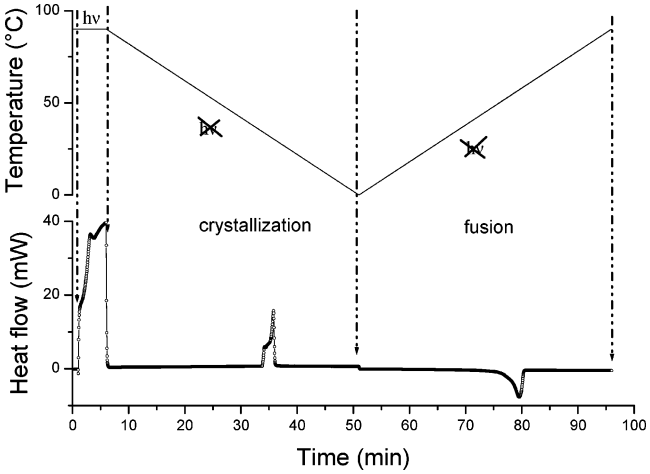

Figure 4. Temperature program used to perform photoDSC experiments. The first stage (1 min) allows the completion of the sample melting. Following is the irradiation period (5 min), the crystallization, and the fusion.

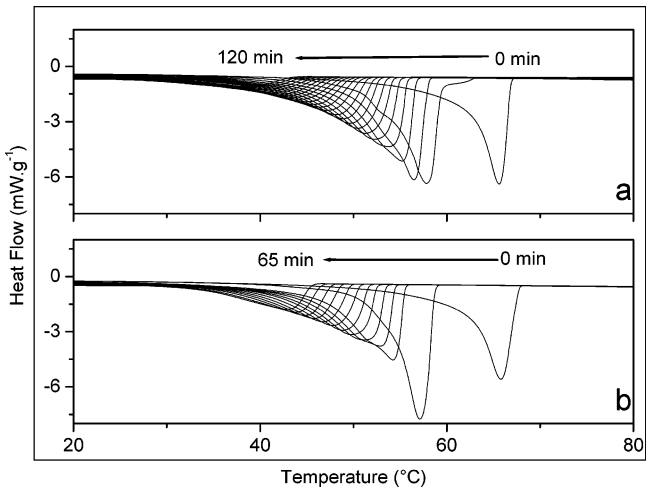

Figure 5. Thermograms of the fusion of the PEO1 sample irradiated at 90 °C and under 500 mW (a) and 750 mW (b) as displayed light intensity values. The exposure time increment was of 5 min and the rate of temperature change 2 °C·min^{-1}.

°C, and the melting endotherm was recorded. A new cycle was then launched with an irradiation time increasing after each cycle.

Only the peak of melting will be studied in this work. Lightpower can be chosen from 0 up to 2000 mW as displayed values. Two power values will be studied here: 750 and 500 mW corresponding to 120 and 80 mW·cm^{-2} actually received by the sample. The calibration of this source has been performed and published in ref 1.

Figure 5 shows typical changes in the melting endotherms of PEO photoaged at 90 °C under the two chosen light intensities. A regular decrease of melting temperature can be observed. Figure 6 shows the variations of the ratio $\Delta H(t)/\Delta H(0)$ with the time of exposure to UV light at different temperatures ranging from 0 to 90 °C. One can observe a progressive decrease of this ratio with increasing irradiation time. However, it is worthy to note that, for the highest temperatures that make PEO completely or partially liquid, the ratio rapidly increases before undergoing a progressive diminution for the longer exposure time.

The evolution of ΔH and T_m can be attributed to the decrease of the molecular weight of PEO, which suggests that chain scissions occur. This interpretation of the thermodynamic

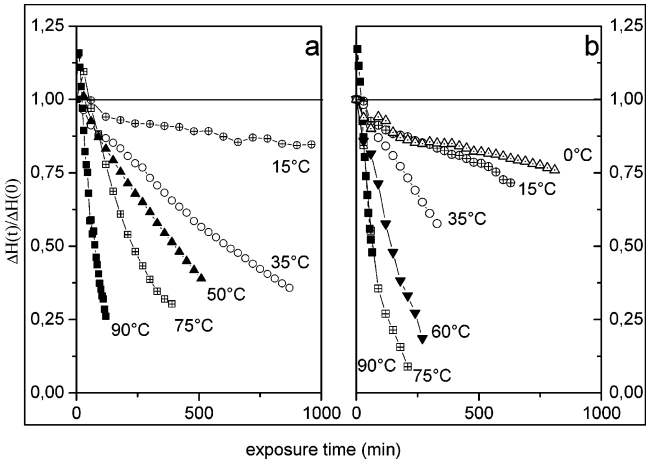

Figure 6. Evolution of the ratio $\Delta H(t)/\Delta H(0)$ versus exposure time for the PEO1 sample irradiated at various temperatures and under 500 mW (a) and 750 mW (b) as displayed light intensity values.

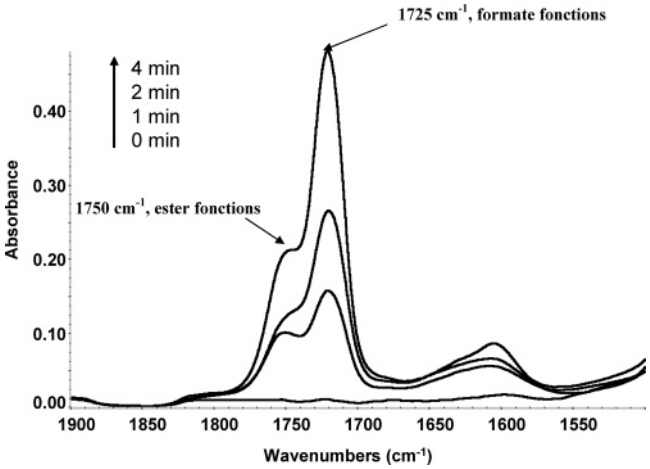

Figure 7. Carbonyl region of photoaged PEO samples irradiated at 750 mW and 75 °C for various times (0, 1, 2, and 4 min). The main band at 1725 cm^{-1} is attributed to formate functions, whereas the shoulder at 1750 cm^{-1} is assigned to esters[9].

measurements is supported by the results of the IR analysis carried out at various exposure times (Figure 7). For these experiments, the aging temperature was 75 °C, and the light intensity was 750 mW. According to ref 9, the absorption band with a maximum at 1725 cm^{-1} and the shoulder around 1750 cm^{-1} were attributed to the formation of formate and ester, respectively. The formation of formate end groups gives evidence of chain scissions.

3. Thermoaging of PEO. Thermal aging experiments were performed by using the same temperature program as shown above in Figure 4 except that light was switched off. Figure 8 shows the endotherms for the material aged at 90 , 75, and 50 °C. The evolutions that are observed are more complex. Indeed, two peaks can be pointed out at 62 and 67 °C, respectively. While thermooxidation proceeds, the peak at 67 °C progressively decreases in favor of the peak at 62 °C before the latter shifts toward the low temperatures. However, as shown in the insets (Figure 8), the ratio of the heat of melting ($\Delta H(t)$) to its initial value ($\Delta H(0)$) reveals the same profile as recorded in the case of photoaging experiments. The only difference is the time scale necessary to produce comparable modifications, which is at least 10 times higher than in the presence of UV light.

To confirm the results of the thermal oxidation experiments, rheological measurements were performed.

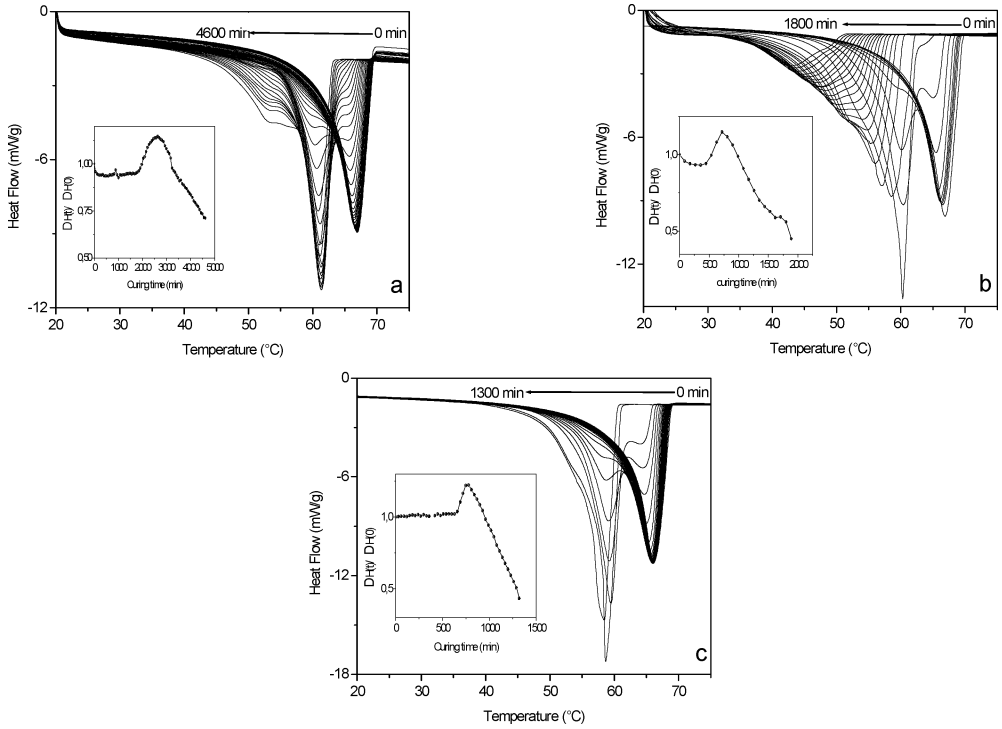

Figure 8. Thermooxidation of PEO1 at 50 °C (a), 75 °C (b), and 90 °C (c). The plots represent the successive DSC endotherms of the fusion of the material. Insets show the evolution of the ratio of $\Delta H(t)$ to $\Delta H(0)$ versus time.

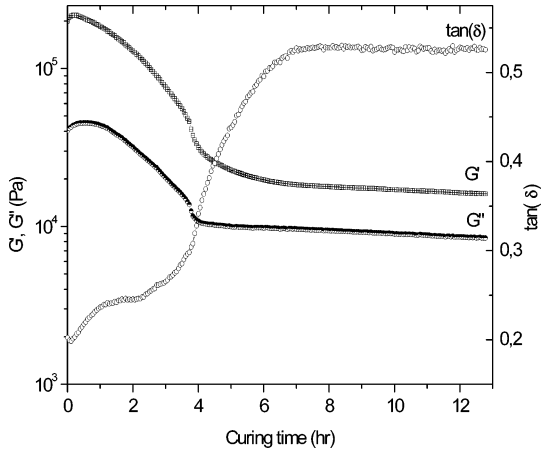

Figure 9. Evolution of the storage modulus (G'), the loss modulus (G''), and the tangent of the phase angle (tan δ) versus time (temperature 90 °C).

In oscillatory measurements of polymer melt flow, the tangent of the phase angle (tan δ) has been used by many authors for characterizing the elasticity and the molecular structure evolution of polymer.[13,14] The tangent of the phase angle describes the balance between the viscous and elastic behaviors in a polymer melt:

$$\tan \delta = G''/G' = \eta'/\eta'' \tag{1}$$

Figure 9 shows the evolution of the elastic modulus (G'), the viscous modulus (G'') and tan δ versus the heating time at 90 °C. The increase of the tan δ signal reveals a loss of elasticity as a consequence of the extend of the chain scissions process. Ferretti et al.[15] already observed the degradation under air by regarding the loss of complex viscosity of PEO as a function of the residence time in a minimixer.

Discussion

In this section, we attempt to show that the kinetic of oxidation can be followed using the photoDSC results. Combining DSC, rheology, XRD, and IRTF gives direct evidences that poly(ethylene-oxide) with a high molecular weight (4×10^6 g·mol^{-1}) undergoes chain scissions in conditions of thermo- and photooxidation. The heat of fusion measured by DSC can be chosen as the valuable parameter related to the chain scissions. As exposed in Figure 2, ΔH increases until the molecular weight reaches 10000−8000 g·mol^{-1} and then decreases continuously. The diminution of ΔH can then be considered as an indicator of the diminution of molecular size from these M_r values.

Figure 10 shows the plot of $\ln(\Delta H(t)/\Delta H(0))$ with the time of oxidation in the dark or under irradiation at two different intensities. A straight line passing through zero can be observed. In these representations, the origin of time was taken at the top of $\Delta H(t)/\Delta H(0)$ curves. The linear variations of $\ln(\Delta H(t)/\Delta H(0))$ suggest that the rate of the global chain scissions reaction follows a first-order kinetic that can be characterized by the following relations:

$$\ln\left(\frac{\Delta H(t)}{\Delta H(0)}\right) = -kt \tag{2}$$

where k is the rate constant of chain scission and t the time of exposure to the aging conditions. Table 2 summarizes the obtained k values for the three DSC experiments.

The theory of the activated complex gives the expression of k:

$$k = \frac{k_B T}{h} \exp\left(-\frac{\Delta G^{\ddagger}}{RT}\right) = \frac{k_B T}{h} \exp\left(\frac{\Delta S^{\ddagger}}{R}\right) \exp\left(-\frac{E_a}{RT}\right) \tag{3}$$

where k_B is Boltzman's constant; h is Plank's constant; $\Delta G^{\ddagger}$, $\Delta S^{\ddagger}$, and E_a are the free enthalpy, the entropy, and the energy

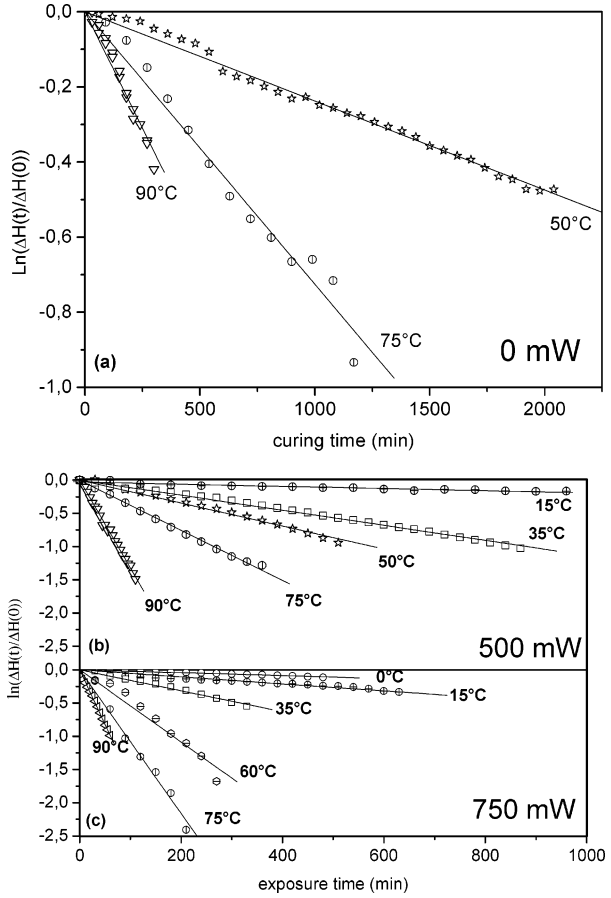

Figure 10. Kinetics of the chain scission reaction occurred in PEO1 at various temperatures. $\Delta H(t)$ is the energy of fusion of the PEO1 after a certain irradiation or cure time (t). The panels represent (a) the thermooxidation and the photooxidation with (b) 500 mW and (c) 750 mW as displayed light intensities which correspond to 80 and 120 mW·cm^{-2}, respectively, as actual received power irradiation.

TABLE 2: The Rate Constants of Chain Scission Occurring in PEO1 Thermooxidized (0 mW) and Photooxidized (500 and 750 mW) at Various Temperatures

0 mW		500 mW		750 mW	
T °C	k min^{-1} × 10^4	T °C	k min^{-1} × 10^4	T °C	k min^{-1} × 10^4
				0	2
		15	2	15	5
		35	11	35	16
50	2	50	17	60	54
75	7	75	38	75	108
90	12	90	132	90	731

of activation, respectively; and R the ideal gas constant. Having performed these experiments at several temperatures, an Eyring's plot, representing $\ln(kh/k_BT)$ as function of the reverse of temperature (T^{-1}), can be drawn.

Figure 11 shows a graphic representation of $\ln(kh/k_BT)$ as a function of $1/T$. The slopes of these straight lines represent $-E_a/R$, whereas their origin ordinates equal $\Delta S^{\ddagger}/R$. For the thermooxidation (0 mW) and the photooxidation experiments (500 and 750 mW), the derived values of $\Delta S^{\ddagger}$ and E_a are listed in Table 3.

The photoDSC experiments indicate that the macromolecular chain scission reaction follows a first-order kinetic law. The photooxidation rate constant was found several times higher than that of thermooxidation. This confirms former results that indicated that the ratio of the amounts of esters and formates were dependent on the experimental conditions of aging, for

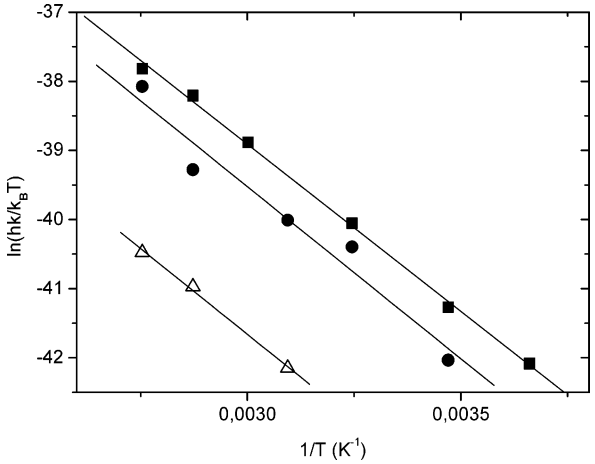

Figure 11. Eyring's plot for the photooxidation (full symbols) and the thermooxidation (empty symbols) of PEO1 (4×10^6 g·mol^{-1}). The square full symbols correspond to a displayed irradiation intensity of 750 mW, and the circle full symbols correspond to 500 mW.

TABLE 3: Activation Energy and Entropy of the Photo- and Thermooxidation of PEO1 (4×10^6 g·mol^{-1})

intensity (mW)	$\Delta S^{\ddagger}$ (J·K^{-1}·mol^{-1})	E_a (kJ·mol^{-1})
0	−222	41.3
500	−204	41.4
750	−203	40.4

example, thermooxidation versus photooxidation of PEO.[9] It has been shown that photooxidation generated five times more formates than esters, whereas thermooxidation gave a 1/1 ratio. The mechanism given in Scheme 1[9] recalls that formates are formed with chain scission, whereas the formation of esters does not involve the cleavage of the macromolecular backbone.

Besides, the activation energies, calculated for both thermal and photooxidation, were found quite identical. The difference in the rate constant values was attributed to the difference in the activation entropies (see Table 3). According to Scheme 1, two kinds of chemical bond can be cleaved, the C−C and the O−O. Scission of the macromolecular chain involves only the homolysis of C−C bonds. However, the cleavage of the C−C bond is resulting from the β-scission of the alkoxy radical **A.** This radical results from the decomposition of a hydroperoxide or a tetroxyde intermediates.[16]

The first-order kinetic law which is deduced from the experiments reported in the paper might be attributed to the cleavage of O−O bonds. To verify this assumption, the kinetics of decomposition of dicumyl peroxide (DCP) were determined. Figure 12 gives details of the experiments that were carried out. A DCP sample (6 mg) was maintained at a chosen decomposition temperature (110, 120, 130, 140, and 150 °C) for 5 min under air atmosphere. After this decomposition time, the sample was quickly cooled (−20 °C/min) down to 0 °C and then heated to the decomposition temperature in order to record the endotherm of fusion ($T_m \approx 40$ °C) and to start a new cycle. Figure 12a shows the results of these experiments performed at 120 °C. The fusion endotherms decrease regularly with the increase of the decomposition time. The area of the fusion endotherm, representing the energy of melting (ΔH), is proportional to the amount of DCP that has not reacted.

The $\ln(\Delta H(t)/\Delta H(0))$ varies linearly with the decomposition time (t) (Figure 12b) revealing that the kinetics of decomposition of DCP follows a first-order law. This permits determining the rate constants that are given in Table 4. Using the results summarized in this table, the Eyring's plots can be drawn as represented in Figure 12c.

SCHEME 1: General Mechanism of the Degradation of PEO[a]

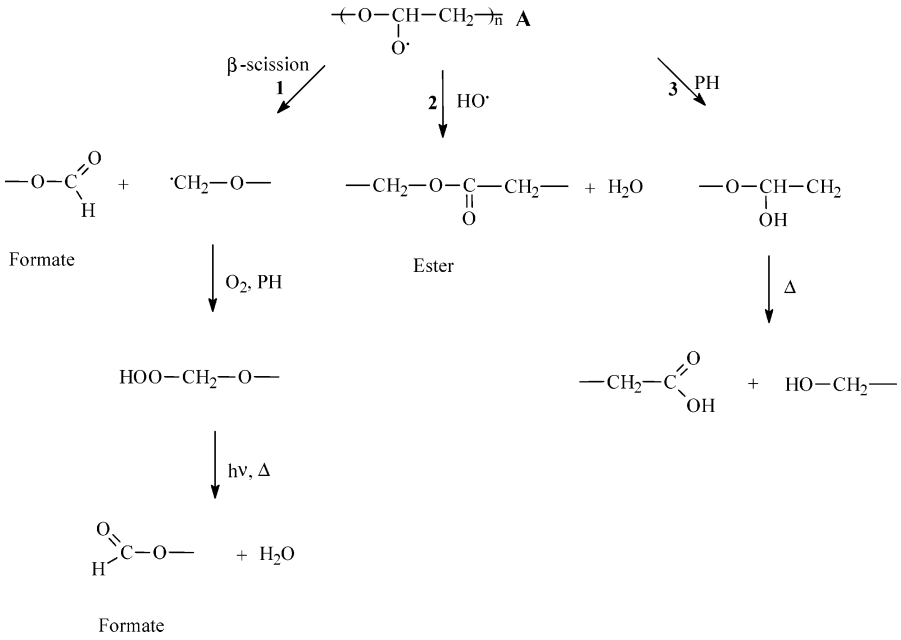

[a] The scheme shows that the chain scissions lead to the formation of the formate, whereas the formation of esters does not involve the cleavage of the macromolecular backbone.

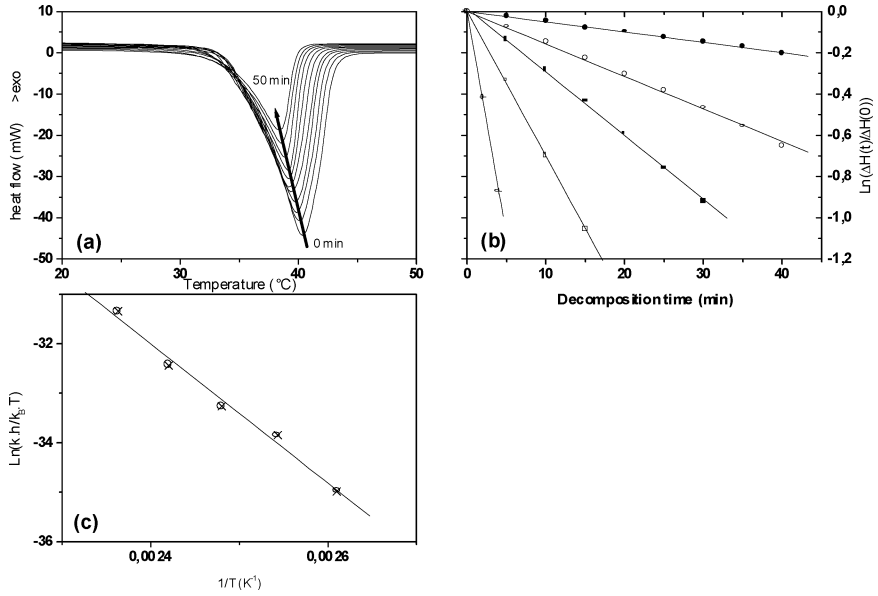

Figure 12. Kinetics of decomposition of dicumyl peroxide followed by DSC. Panel a represents successive endotherms of the fusion. After each fusion, the sample was heated for 5 min at 120 °C. The same experiment was performed at 110, 120, 130, 140, and 150 °C. Panel b shows $\ln(\Delta H(t)/\Delta H(0))$ vs $1/T$ plotted for the various temperatures. The slopes of these plots give the rate of the decomposition reaction. Panel c shows Eyring's plots. The slopes of theses straight lines give the activation energies.

TABLE 4: Constants of the Decomposition Rate of DCP at Various Temperatures

T °C	*K* $\text{min}^{-1} \times 10^4$
110	49.8
120	157.5
130	301.4
140	700.2
150	2157.0

The activation energy of DCP decomposition that can be deduced was found equal to 117 kJ/mol. This result is in a good agreement with the published activation energy values for such peroxide structures.[17]

Activation energies accounting for the decomposition of peroxidic structures have been obtained and published for various macromolecular peroxides. The values range between 120 and 160 kJ/mol.[18]

The activation energies determined in the present study (41 kJ·mol^{-1}) are too low to fit these reactions of decomposition. However, no general and convincing explanation can be proposed. Additional experiments planned in our group are necessary, with the objective of elucidating the role of the diffusion processes, for instance.

Conclusion

The main objective of this work was to demonstrate that photoDSC is suitable to study the oxidative behavior of

semicrystalline polymers. The photoDSC apparatus was used to study photooxidation and thermooxidation of a high molecular weight poly(ethylene oxide) (PEO). The changes in the enthalpy of fusion of PEO were used as an experimental parameter that is related to the length of the macromolecular chains. IR and rheological measurements have been performed to confirm that the modifications resulting from photo and thermal aging produced in situ in the DSC equipment revealed the chain scission phenomena. It was found that the chain scission reactions undergone by PEO follow a first-order kinetic law. The activation energies for both thermo- and photooxidation reactions were found identical and equal to 41 kJ/mol. The activation energy for cleavage of the −O−O− bond in dicumyl peroxide was measured and estimated as 117 kJ/mol. This suggests that the cleavage of the alkoxy peroxide which is involved in the commonly proposed reaction mechanism could not be the determining stage in the global kinetics of chain scissions.

References and Notes

(1) Morel, M.; Lacoste, J.; Baba, M. *Polymer* **2005**, *46*, 9274−9282.
(2) Shieh, Y.-T.; Lui, G.-L.; Hwang, K. C.; Chen, C.-C. *Polymer* **2005**, *46*, 10945−10951.
(3) Sun, L.; Zhu, L.; Ge, Q.; Quirk, R. P.; Xue, C.; Cheng, S. Z. D.; Hsiao, B. S.; Avila-Orta, C. A.; Sics, I.; Cantino, M. E. *Polymer* **2004**, *45*, 2931−2939.
(4) Da Costa, V. M.; Fiske, T. G.; Coleman, L. B. *J. Chem. Phys.* **1994**, *101* (4), 2746−2751.
(5) Miyazawa, T.; Fukushima, K.; Ideguchi, Y. *J. Chem. Phys.* **1962**, *37* (12), 2764−2776.
(6) Porto, A. O.; Silva, G. G.; Magalhaes, W. F. *J. Polym. Sci., Part B: Polym. Phys.* **1999**, *37*, 219−226.
(7) Harris, J. M. *Poly(ethylene glycol) Chemistry: Biotechnical an Biomedical Application;* Plenum Press: New York, 1992.
(8) Blin, J. M.; Leonard, A.; Yuan, Z.-Y.; Gigot, L.; Vantomme, A.; Cheetham, A. K.; Su, B. L. *Angew. Chem., Int. Ed.* **2003**, *42*, 2872.
(9) Morlat, S.; Gardette, J.-L. *Polymer* **2004**, *42*, 6071−6079.
(10) Wilhem, C.; Gardette, J. L. *Polymer* **1998**, *39*, 5973−5980.
(11) Homming, D.; Goderis, B.; Dolbnya, I.; Reynaers, H.; Groeninckx, G. *Polymer* **2005**, in press.
(12) Brotel, E.; Hodorowicz, S.; Lamot, R. *Makromol. Chem.* **1979**, *180*, 2491−2498.
(13) Lee, Y. J.; Sohn, H. S.; Park, S. H. *Korea-Australia Rheol. J.* **2000**, *12*, 181−186.
(14) Kumar, A.; Commereuc, S.; Verney, V. *Polym. Degrad. Stab.* **2004**, *85*, 751−757.
(15) Ferretti, A.; Carreau, P. J.; Gerard, P. *Polym. Eng. Sci.***2005**, *45* (10), 1385−1394.
(16) Phillipart, J. L.; Gardette, J. L. *Polym. Degrad. Stab.* **2001**, *71*, 189−194.
(17) Gugumus, F. *Polym. Degrad. Stab.* **2000**, *69*, 23−34.
(18) De, P.; Chattopadhyay, S.; Madras, G.; Sathyanarayana, D. N. *Journal of Applied Polymer Science* **2002**, *86*, 957−961.